Electrochemical Reduction of CO_2 on Au Electrocatalysts in a Zero-Gap, Half-Cell Gas Diffusion Electrode Setup: a Systematic Performance Evaluation and Comparison to an H-cell Setup

Shima Alinejad [a], Jonathan Quinson [b], Gustav K. H. Wiberg [a], Nicolas Schlegel [a], Damin Zhang [a], Yao Li [c], Sven Reichenberger [c], Stephan Barcikowski [c], Matthias Arenz *[a]

[a] University of Bern, Department of Chemistry, Biochemistry and Pharmaceutical Sciences, Freiestrasse 3, 3012 Bern, Switzerland
[b] University of Copenhagen, Department of Chemistry, Universitetsparken 5, 2100 Copenhagen Ø, Denmark
[c] University of Duisburg-Essen, Technical Chemistry I and Center of Nanointegration Duisburg-Essen (CENIDE), Universitätsstraße 7, Essen, North Rhine-Westphalia, 45141, Germany

*Corresponding Author
E-mail: matthias.arenz@dcb.unibe.ch

Abstract

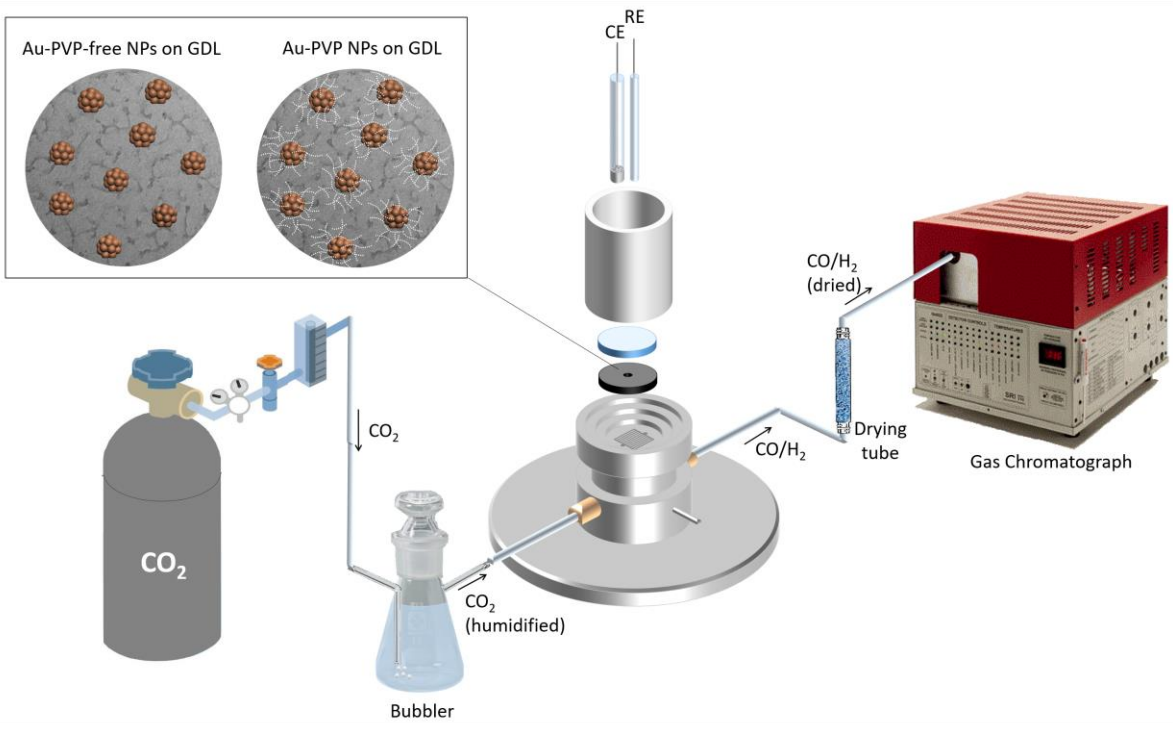

Much research effort has been devoted to the development of effective catalysts for the electrochemical reduction of CO_2 (CO2RR). For CO2RR, the most common catalyst screening method is performed in an H-cell configuration where the reactant CO_2 gas is usually dissolved in an aqueous bicarbonate-based electrolyte. However, the low solubility of CO_2 in aqueous solutions (~35 mM at 298 K and 1 atm pressure) causes mass transport limitations in such setups. Based on H-cell measurements gold (Au) is one of the most selective catalysts for the CO2RR to CO. The preparation of small Au nanoparticles (NPs) based on conventional synthesis methods often requires the use of surfactants and capping agents such as polyvinylpyrrolidone (PVP). Here, we present a systematic evaluation of the performance of Au NPs for the CO2RR in our recently developed gas diffusion electrode (GDE) setup and compare the results to investigations in a conventional H-cell configuration. The GDE setup can be characterized as a zero-gap, half-cell setup and supplies a continuous CO_2 stream at the electrode−membrane electrolyte interface to circumvent CO_2 mass transport limitations encountered in conventional H-cells. By using surfactant-free, laser-generated Au NPs, we investigate the influence of the catalyst loading as well as the influence of PVP addition. The results comparing the two screening methods show that the performance of the same catalyst can be substantially different in the different setups, which highlights the importance of having commercially relevant conditions for catalyst screening. In both setups, it is found that the presence of PVP favours the hydrogen evolution reaction (HER), however, in the GDE setup PVP is more detrimental for the performance than in conventional H-cells.

1. Introduction

The electrochemical reduction of CO_2 (CO2RR) into value-added products such as fuels and chemicals is considered an important contribution for curbing the use of fossil fuels and consequently diminishing atmospheric emissions of CO_2[1]. In the presence of an active and selective heterogeneous or homogeneous catalyst, CO_2 can be reduced towards carbon monoxide, formate, methanol, and other higher-value carbon-coupled products. These products can be used as feed-stocks for chemical synthesis or converted into hydrocarbon fuels[2]. Among these products, carbon monoxide (CO) is one of the main target products of CO2RR because syngas (H_2 and CO) is widely used in current industrial processes[3]. Achieving a high activity and selectivity is crucial for the technological and economic viability of the CO_2 electroreduction process. Low cell overpotentials ($|\eta_{cell}| < 1$ V), a CO-related current density of $j_{CO} > 150$ mA cm^{-2} and faradaic efficiency (FE) for CO ($FE_{CO} > 75\%$) are required for the economic viability of the CO2RR[4] and remain a challenge even after almost two decades of research[5–7]. The origin of the low current densities reported cannot solely be attributed to the low performance of the used CO_2 electroreduction catalysts but also can be related to the employed screening method used for the catalytic testing itself. The most common catalyst screening method for CO2RR is based on H-cell experiments in which the CO_2 reactant gas is dissolved in an aqueous bicarbonate-based electrolyte[8]. In such a setup, the low solubility of the CO_2 reactant gas in aqueous solutions (~35 mM at 298 K and 1 atm pressure)[7] causes mass transport limitations for the preferred CO product, whereas the reactant for the unfavored evolution of H_2 gas (i.e. water) is not mass transport limited. Therefore, in traditional testing configurations, the total measured current densities are substantially lower than the commercially relevant current densities ($j_{tot} > 200$ mA cm^{-2})[9]. As a consequence, several different setups have been introduced that overcome CO_2 mass

transport limitations by supplying a continuous CO_2 stream at the electrode−electrolyte interface in GDE flow electrolyzers[4,10,11]. Among these different types of GDE setups, gas-fed approaches which are known as catholyte free or zero-gap electrolyzers are recognized as the most promising because of their similarity to polymer electrolyte fuel cell technologies[12,13].

Yet, as indicated previously, also the available catalysts still limit the CO2RR performance. According to H-cell measurements, Au is one of the most selective catalysts for CO2RR to CO[14]. In conventional synthesis methods, such as the chemical reduction of precursors[15] and wet impregnation[16], the presence of stabilizers, ligands, and reducing agents and/or support is necessary for the synthesis of the catalyst. Typically, surfactants and capping agents are used for the preparation of small colloidal Au NPs[17]. Polymeric materials, mainly polyvinylpyrrolidone (PVP), are applied as capping and/or stabilizing agents for synthesizing NPs in the liquid phase[18]. Using PVP in colloidal synthesis leads to NPs with controlled composition and structural features. Depending on the synthetic conditions, PVP can play the role(s) of a surface stabilizer, growth modifier, nanoparticle dispersant, and/or reducing agent. The amphiphilicity and the molecular weight of PVP can affect NP growth and morphology by providing different solubility in diverse solvents, preferential growth of selected crystal facets, and even access to kinetically controlled growth conditions[19]. In this respect, it must be mentioned that due to the high level of toxicity and low biodegradability of synthetic surfactants, these materials have negative impacts on the environment such as ruining aquatic microbial populations, damaging aquatic life, reducing photochemical energy conversion efficiency of plants, and detrimentally affecting waste-water treatment processes. Considering that roughly 60% of the global usage of surfactants, which is over 15 million tons, winds up in the aquatic environment, it is imperative to act urgently for

finding alternative ways of shaped-control catalyst synthesis[20]. In addition, albeit surfactants ease the route of shaped-control catalyst synthesis, depending on the interaction between the surfactants and surface of the NPs, surfactants can strongly influence NPs catalytic properties[21–23]. The protection of the catalyst surface by surfactants can lead to both catalyst poisoning and deactivation[24] or improved selectivity for the desired products[23,25,26]. For instance, if the binding between the capping agent and metal surface is too strong, the reactivity of the metal NPs remarkably diminishes. On the other hand, the presence of the ligands can also electronically alter a too-strong adsorption strength (enthalpy) of products and educts optimal or block undesired adsorption configurations and thereby affect the oxidation of specific functional groups in the reactant molecule[23,25,26]. To study which of this broad spectrum of influences and possible cross-correlations a surfactant induces on the catalytical properties of surfactant-free NPs are required[23]. Considering the superior role of the shape-controlled NPs in electrocatalysis, the most critical issue is to either establish a synthesis strategy for surfactant-free nanoparticles or a post-treatment strategy to remove the capping agents and surfactants from the particle surfaces without any alteration of particle size, morphology, etc. For surfactant or capping agent removal from the surface of NPs, various strategies have been developed in the last years[27–29], however, a facile method to clean the surface of the NPs remains challenging. As an example, thermal treatment can lead to the loss of the surface orientation and agglomeration of the NPs[30]. Generally, the simple removal of PVP molecular impurities considerably alters nanoparticle size, shape, and formation kinetics[31] and it requires energy and time-consuming steps[32]. Hence to circumvent this drawback, in this study we used pulsed laser ablation in liquids (PLAL) to directly synthesize surfactant-free Au colloidal NPs[23,33,34], here referred to as Au-PVP-free NPs.

Afterward, the Au-PVP-free NPs batch was split into two parts. One batch was kept as is, while PVP was added to the other batch, here referred to as Au-PVP NPs. Consequently, the Au-PVP-free and Au-PVP colloidal NPs come from the same source and they have the same particle size avoiding the influence of particle size effects during the measurements. This way, the laser-generated Au NP can act as a surfactant-free reference catalyst similar to previous studies[35].

One of the objectives of the presented work was to investigate the influence of PVP on the catalyst performance in different reaction environments, i.e., a GDE setup with high reactant mass transport and a conventional H-cell with limited CO_2 mass transport. We employed our recently introduced GDE setup[8,36] that originally has been designed for the application in fuel cell research[37] and can be characterized with respect to its application for the CO2RR as a zero-gap, half-cell GDE setup. In this setup, a humidified CO_2 stream is continuously fed through the GDE cell, adjacent to the catalyst film to circumvent CO_2 mass transport limitations. To characterize the performance in the GDE setup, we performed the same potentiostatic CO_2 electrolysis experiments in the GDE and an H-cell setup and compared the results. For all investigated catalyst layers in this study, the H-cell configuration favors higher FE_{CO}. Then we investigated the influence of the catalyst loading in the GDE setup, and in the next step, we investigated the influence of PVP on the performance. We observed that the performance of the same catalyst under same experiment conditions can be substantially different.

2. Experimental

2.1. Chemicals, Materials, Gases, and Instruments

For the preparation of the catalyst ink, isopropanol (IPA, 99.7+%, Alfa Aesar) and a Nafion ionomer (D1021, 10 wt% in H_2O, EW 1100, Fuel Cell Store) were used. For the electrolyte

preparation, the membrane activation, and the GDE cell cleaning the ultrapure Milli-Q water (resistivity > 18.2 MΩ cm, total organic carbon (TOC) < 5 ppb) from a Milli-Q system (Millipore IQ7000) was used. Potassium hydroxide (KOH, Merck) and Potassium bicarbonate ($KHCO_3$, ACS grade, Sigma-Aldrich) were used for the electrolyte preparation. An Anion exchange membrane (Sustainion® X37-50 Grade RT Membrane, with a dry thickness of 50 µm thick, Dioxide Materials) and gas diffusion layers (GDL) with a microporous layer (MPL, H23C8, 200 µm thick @ 1MPa, Freudenberg) and without a microporous layer (H23, 170 µm thick @ 1MPa, Freudenberg) were employed in the GDE measurements. H_2 (99.999%), CO_2 (99.999 %), and calibration standard gas from (Carbagas, Switzerland) were used in the electrochemical measurements. A gas chromatograph (Model 8610C, SRI Instruments) equipped with a thermal conductivity detector (TCD) and a flame ionization detector (FID) coupled to a methanizer were used to detect hydrogen and carbon monoxide, respectively. To avoid damage of the GC column, the outlet gas of the CO2RR cell was passed by a drying tube to remove the excess water (Cole-Parmer Drierite, Fisher Scientific) before reaching the sample loop of the GC. The gas flow rate was controlled and measured during the CO_2 electrolysis by two flow meters (universal flow meter 7,000 GC by Ellutia and Q-Flow 140, FLQ-CTSS-BK-M, CONTREC AG).

2.2. Synthesis of Au-PVP-free and Au-PVP colloidal nanoparticles

2.3. In order to generate the Au colloidal NPs, a ns-laser system (EdgeWave IS-400-L) and a continuous-flow ablation chamber were used[38] (Figure S1a-b). For generating the particles, the laser beam was focused onto the bulk Au target surface (0.5 mm thick foil, 99.99% purity, AGOSI) and moved by a galvanometric scanner system (Sunny S-8210D) at 2 m s^{-1} scan speed in a

rectangular pattern. To focus the laser onto the target, the scanner was equipped with an F-Theta lens (f=100 mm). The working distance between the lens (surface) and the target was set to 115 mm to maximize nanoparticle productivity. Milli-Q water (> 18.2 MΩ cm) containing 500 µM NaCl was pumped through the ablation chamber with a flow rate of 100 mL min^{-1} during ablation. The added NaCl in micromolar concentration is a well-known size-quenching agent for laser-generated colloidal gold nanoparticles where the chloride improves the electrostatic stabilization and hence quenches nanoparticle growth directly during laser sythesis[39]. A nanoparticle productivity of 1 g h^{-1} which is in line with previous studies on laser ablation with nanosecond-pulsed IR lasers[38] was calculated from the ablation time and a differential weighting of the target before and after ablation. With the given flow rate, the gained concentration of Au nanoparticles was 160 mg L^{-1}. To remove residual size fractions larger than 10 nm, the laser-generated colloids were continuously size-separated by a tubular bowl centrifuge (CEPA LE GP) with a rotation speed of 40,000 rpm and a colloid volume flow rate of 50 mL min^{-1}. The desired small size fraction of the Au-PVP-free colloid was obtained with a concentration of 37.5 mg L^{-1} measured by inductively coupled plasma-mass spectrometry (ICP-MS) and used for further experiments. The main advantage of using a tubular bowl centrifuge is that a large volume of the colloid can continuously be processed without interruption[38]. The hydrodynamic particle size distribution of the initial laser-generated Au colloid and the small fraction after continuous centrifugation determined by analytical disc centrifugation are shown in Figure S1c-d. The Au-PVP-free colloid batch was split into two parts. One part was kept as is (Au-PVP-free), while a 0.9 mM PVP solution (Arcos Organics, 3500 g mol^{-1}) was added to 6 L Au colloid under constant mixing (Au-PVP, 0.15 mM).

The primary particle size of the separated particles is verified by transmission electron microscopy (TEM) and small angle x-ray scattering (SAXS) (Figure 1).

2.4. Preparation of the Catalyst Ink

13.2 mL of the colloidal Au suspension (= 0.5 mg of Au) and 2.6 µL of the 10 wt.% Nafion dispersion was mixed with 13.2 mL of IPA. The glass vial containing the mixture was sonicated in an ultrasonic bath for 15 min. For the ink preparation, two types of ionomer dispersions, i.e., a Nafion ionomer and an Anion ionomer (Sustainion XA-9 Alkaline Ionomer 5% in ethanol, Dioxide Materials) were examined (Figure S2 and S3). The Anion ionomer caused particle agglomeration especially for the Au-PVP-free ink, resulting in a color change of the colloidal dispersions from red to purple. Results of ultraviolet–visible (UV-Vis) spectroscopy (Figure S4) indicate that adding the Nafion ionomer to the Au-PVP-free or Au-PVP colloidal suspensions does not cause any interaction with the NPs as the UV-Vis peak position does not shift. Therefore, Nafion ionomer was chosen for the ink preparation. The UV-Vis spectra recorded upon adding Anion ionomer into the ink (Figure S5), indicate that the presence of the PVP prevents the interaction between ionomer and NPs.

2.5. Preparation of the Catalyst Film

For the preparation of the catalyst films, a vacuum filtration setup was used (Figure S6). In this setup, a cylindrical reservoir with a cross-sectional area of 1.76 cm^2 was placed on top of the GDL, which was positioned onto a fritted glass filter. All this was placed on a collecting bottle. The reservoir was filled with 9.45 or 2.36 mL of ink and afterward, vacuum was applied with the help

of a Schlenk line pump. By slowly sucking the ink through the GDL, a homogenous catalyst layer was obtained, which was dried overnight in air. The theoretically obtained Au loading of the thus prepared GDE is 100 μg_{Au} cm^{-2} (for 9.45 mL of ink) and 25 μg_{Au} cm^{-2} (for 2.36 mL of ink). As the colloidal Au NPs were not supported, a loss of particles during the vacuum filtration process was expected. Therefore, for the determination of the real catalyst loading, inductively coupled plasma-mass spectrometry (ICP-MS) of freshly prepared and dissolved samples (see description below) was performed (Table 1). As the vacuum filtration process and the film preparation of the Au-PVP GDEs were the same as for the Au-PVP-free GDEs, we expect the same loading for Au-PVP GDEs. However, because of presence of PVP in the Au-PVP GDEs, it was not possible to perform a reliable ICP-MS analysis. In the following, the samples will be defined by the catalyst loading as evaluated by ICP-MS.

Table1. Determined Au loadings of Au-PVP-free GDEs.

Type of GDE	**Theoretical Au loading (μg_{Au} cm^{-2})**	**Measured Au loading based on ICP-MS analysis (μg_{Au} cm^{-2})**
Au-PVP-free	25	10 ± 1
Au-PVP-free	100	50 ± 1

2.6. Preparation of Working Electrodes (WE)

From the GDE, a WE with a circular diameter of Ø 3 and 5 mm was punched and inserted into the GDE setup and H-cell, respectively. For the GDE setup, one GDL without and one with MPL (micro porous layer) (Ø 2 cm) was used, respectively. To assemble the GDE, a hole of Ø 3 mm in the

center that was filled with the Ø 3 mm GDE, and an activated Anion membrane (Ø 2 cm) was placed between the upper cell body (polytetrafluoroethylene, PTFE) and the lower cell body (stainless steel). For the activation of the Anion membrane, it was previously immersed in 1 M KOH for 24 h and thereafter punched into circles with a diameter of 2 cm. The punched and activated membranes were stored in 1 M KOH. Before assembling the membrane into the GDE setup, it was thoroughly rinsed with ultrapure Milli-Q water and thereafter dried with precision wipes (Kimtech science). For the preparation of the WE for the H-cell, a rectangular piece (0.8 cm × 3 cm) of a GDL with an MPL was used. The backside and the edges of the electrode were masked with Teflon tape thus leading to an exposed surface area of Ø 5 mm, where the punched Ø 5 mm GDE was placed. Although glassy carbon is more common as a WE for H-cell measurements, here we used a GDL to have the same porosity and properties as the GDE setup. So doing, we can have a fairer comparison between the results of the GDE setup and the H-cell setup.

2.7. Preparation of the GDE setup

Our recently introduced GDE setup was employed in this study[8,36,37]. As described above, the WE in the form of a GDE was placed on top of the flow field in the stainless-steel lower cell body and an activated Anion exchange membrane was placed on top of the GDE to separate the liquid electrolyte from the catalyst layer. The PTFE upper cell body was placed above the Anion membrane and pressed to the lower cell body by means of a stainless-steel clamp and then it was filled with 15 mL of 2 M KOH (pH≈14). A silver/silver chloride electrode (Ag/AgCl, 3 M KCl, VWR, double junction design) and a gold wire were used as a reference electrode (RE) and a counter electrode (CE), respectively. For improving the reproducibility of the measurements, the

CE was placed inside a glass capillary with a glass frit on the bottom to avoid the trapping of gas bubbles in the Teflon cell. All potentials in this study are referred to the RHE potential based on the following formula $E_{RHE} = E_{Ag/AgCl} + E^0_{Ag/AgCl} + 0.059 \times pH$ (in volts). We used the pH values of bulk electrolyte, 0.5 M $KHCO_3$ in the H-cell (pH≈7.2) and 2 M KOH in the GDE setup (pH≈14), for the RHE conversions. Moreover, the resistance between the WE and RE and the applied electrode potentials was monitored online using an AC signal (5 kHz, 5 mV). The cleaning of the cell was same as our previous works[40,41]. A glass bubbler was connected to the gas inlet of the lower cell body to humidify the gas. During electrolysis, a humidified CO_2 stream (16 mL min^{-1}) was continuously fed through the inlet of the GDE setup to transport the gaseous products from the outlet of the GDE setup to the sample loop of the GC.

2.8. Preparation of the H-cell setup

A custom-built gas-tight H-type glass cell with a proton exchange membrane (Nafion 117, Sigma Aldrich) separating the catholyte and the anolyte was used in this study. Both cathodic and anodic compartments were filled with 30 mL of 0.5 M $KHCO_3$ (pH≈7.2) electrolyte. The described WE (section 2.5) and a single junction Ag/AgCl (saturated KCl, Pine Research) as RE were placed in the cathodic compartment. A Pt foil (0.8 cm × 2 cm) as CE was placed in the anodic compartment. Prior to the CO_2 electrolysis, both cathodic and anodic compartments were saturated with CO_2 (13 mL min^{-1}) for 30 min. The CO_2 flow enabled the transport of gaseous products from the headspace of the catholyte to the sample loop of the GC.

2.9. CO_2 Electrolysis Experiment

Potentiostatic CO_2 electrolysis experiments were carried out for 1 h at the selected applied electrode potentials using a potentiostat (ECi-200, Nordic Electrochemistry Aps). The outlet gas of the cell was continuously flowing through the gas chromatograph (GC), and at a certain period of time, every 10 min, the analysis of gaseous products was carried out by online GC triggered by the potentiostat. The GC was calibrated before mesurements with a calibration standard gas mixture (Carbagas, Switzerland) containing all products (CO and H_2). A fresh WE was used for each experiment to prevent the possible influence of catalyst layer degradation on the product distribution. The control file program of the GC and a representive chromatogram of a GC analysis are given in figure S7 and S8.

The Faradaic efficiency (FE) for a given gaseous product i was determined based on equation (1):

$$FE_i = \frac{j_i}{j_{total}} = \frac{C_i . v . z . F}{10^6 V_m . j_{total}} \quad (1)$$

where j_i represents the partial current for the conversion of CO_2 into the product i, C_i resemples the concentration of product i in ppm measured by online GC, v is the gas flow rate, z is the number of electrons involved in the formation of the particular product, F represents Faraday's constant, V_m is the molar volume of of ideal gas at ambient condition (22.4 L mol^{-1}), and j_{total} the total current at the time of the injection of the gas into the sample loop of the GC.

2.10. Ultraviolet–Visible (UV-Vis) Extinction Spectroscopy

The Au-PVP-free and Au-PVP colloidal suspension and catalyst ink before and after Anion and Nafion ionomer addition were measured by UV/Vis extinction spectroscopy (Thermo Scientific GENESYS 10S UV-Vis Spectrophotometer) in a glass cuvette with 10 mm path length.

2.11. Inductively Coupled Plasma-Mass Spectrometry (ICP-MS)

A WE with a circular diameter of Ø 3 and loaded with freshly prepared Au-PVP-free and Au-PVP catalysts (GDEs) was placed in a glass test tube. The test tube was kept in a water bath at 60 °C under vigorous stirring. After the addition of 5 mL aqua regia into the tube, the latter was quickly closed for 1 hour with the help of a stopper. In this way, the reaction of the hydrochloric acid (HCl 37%, Grogg Chemie) and nitric acid (HNO_3 65%, Merk) could take place inside while containing the vapor inside to quantitatively dissolve the Au NP film on the GDE. The resulting solution was diluted by factors of 100, 50, and 30 with 3% HNO_3 and was then fed into a NExION 2000 ICP−MS instrument (PerkinElmer) to determine the Au mass loading of the electrodes.

2.12. Transmission Electron Microscopy (TEM)

The Au NP colloids were dropped on a TEM grid and were analyzed using a Jeol 2100 TEM microscope operated at 200 kV. The size of the nanoparticles was evaluated using the ImageJ software and the average diameter was evaluated from at least 200 individual nanoparticles from different micrographs to ensure that they are representative for the sample.

2.13. Small Angle X-ray Scattering (SAXS)

The colloidal Au NPs were also characterized by SAXS following the general procedure and methods detailed elsewhere[42]. In short, the Au NP colloids were placed in dedicated capillaries and measured using a SAXSLab instrument at the Niels Bohr Institute at the University of Copenhagen. The background used for measurements was MilliQ water.

2.14. Scanning Electron Microscopy and Energy-Dispersive X-ray Spectroscopy

The cross-sectional characterization of the prepared catalyst films of 50 μg_{Au} cm^{-2} of Au-PVP-free and Au-PVP GDEs was carried out with scanning electron microscopy (SEM) imaging. The analysis was conducted with a Zeiss Gemini 450 scanning electron microscope with both InLens secondary electron detectors. An accelerating voltage of 2 kV and a current of 200 pA were applied at a working distance of 4 mm. The use of imaging coupled to energy-dispersive X-ray analysis (EDX) analysis made it possible to track the stabilization of Au NPs on top of the GDL. The AZtec 4.2 software (Oxford Instruments) was used to acquire EDX spectra and surface mappings of the GDEs. An acceleration voltage of 20 kV and a current of 200 pA were applied at a working distance of 8.5 mm.

2.15. Raman Spectroscopy

Raman spectra were collected by a LabRAM HR800 confocal microscope (Horiba Jobin Yvon, Germany). The spectra were acquired using a 100x objective lens (MPLFLN, Olympus, Japan) and a 532 nm laser source for excitation (16 mW, torus 532, Laser Quantum, UK). The backscattered light was dispersed by an 1800 line/mm grating and subsequently detected by a 1024 x 256 pixel CCD detector at a temperature of -59 °C. For calibration, a silicon wafer standard (520.6 cm^{-1}) was used.

3. Results and Discussion

As mentioned in the introduction one of the objectives of this study was to compare the performance of Au-PVP-free NPs and Au-PVP NPs towards the CO2RR. The representative TEM

micrographs of the as-prepared Au-PVP-free and Au-PVP NPs, and particle size distributions derived from the TEM and SAXS analysis for these two Au NP colloids are given in Figure 1. As expected, (both samples are aliquotes of the same batch) similar particle size of ~6 nm is observed within the error margin for both samples. Yet, a very high deviation of about 6 nm was observed for the PVP-containing sample. This deviation was linked to particularly large black "chunks" observed in the TEM images (Figure 1-d) that were included in the size determination to avoid systematic exclusion of potentially large Au NPs and led to a tail to larger particle sizes in the particle size histogram. Yet, it is more likely that these "chunks" can be attributed to dried PVP on the TEM grids since the Au-PVP colloidal suspension potentially still contained free PVP. SAXS measurements were additionally performed on the colloidal dispersions (without the need for drying) to validate the size distribution obtained by TEM. The retrieved probability density function derived from SAXS analysis indicates a narrower size distribution than evaluated by TEM when PVP was used with a size around 6.2 ± 1. 9 nm, Figure 1-f. Consequently, we can investigate the effect of PVP on the CO2RR without the potential influence of a particle size effect.

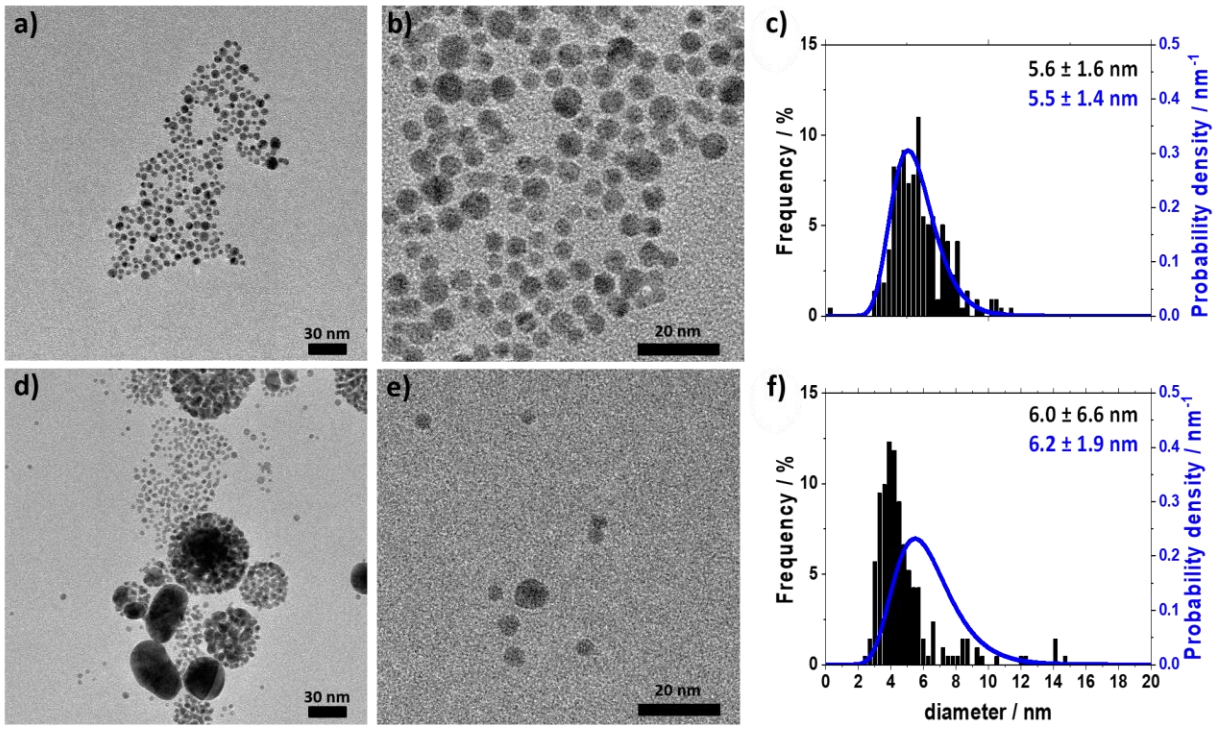

Figure 1. Representative TEM micrographs recorded at different magnifications showing Au-PVP-free (a and b), and Au-PVP (d and f) colloidal NPs. The particle size distribution derived from the TEM (black, left Y-axis), and SAXS analysis (blue, right Y-axis) for Au-PVP-free (c), and Au-PVP (f) colloid NPs.

In addition to the colloidal NPs, we characterized the as-prepared GDEs by SEM and EDX. In Figure 2 representative cross-sectional SEM images of the prepared GDE's including EDX mapping are shown for as-prepared Au-PVP-free and Au-PVP GDEs with a loading of 50 μg_{Au} cm^{-2}. The imaging indicates that for both, the Au-PVP-free and the Au-PVP GDEs, the Au NPs are deposited on top of the MPL of the GDL and they do not permeate into the GDL.

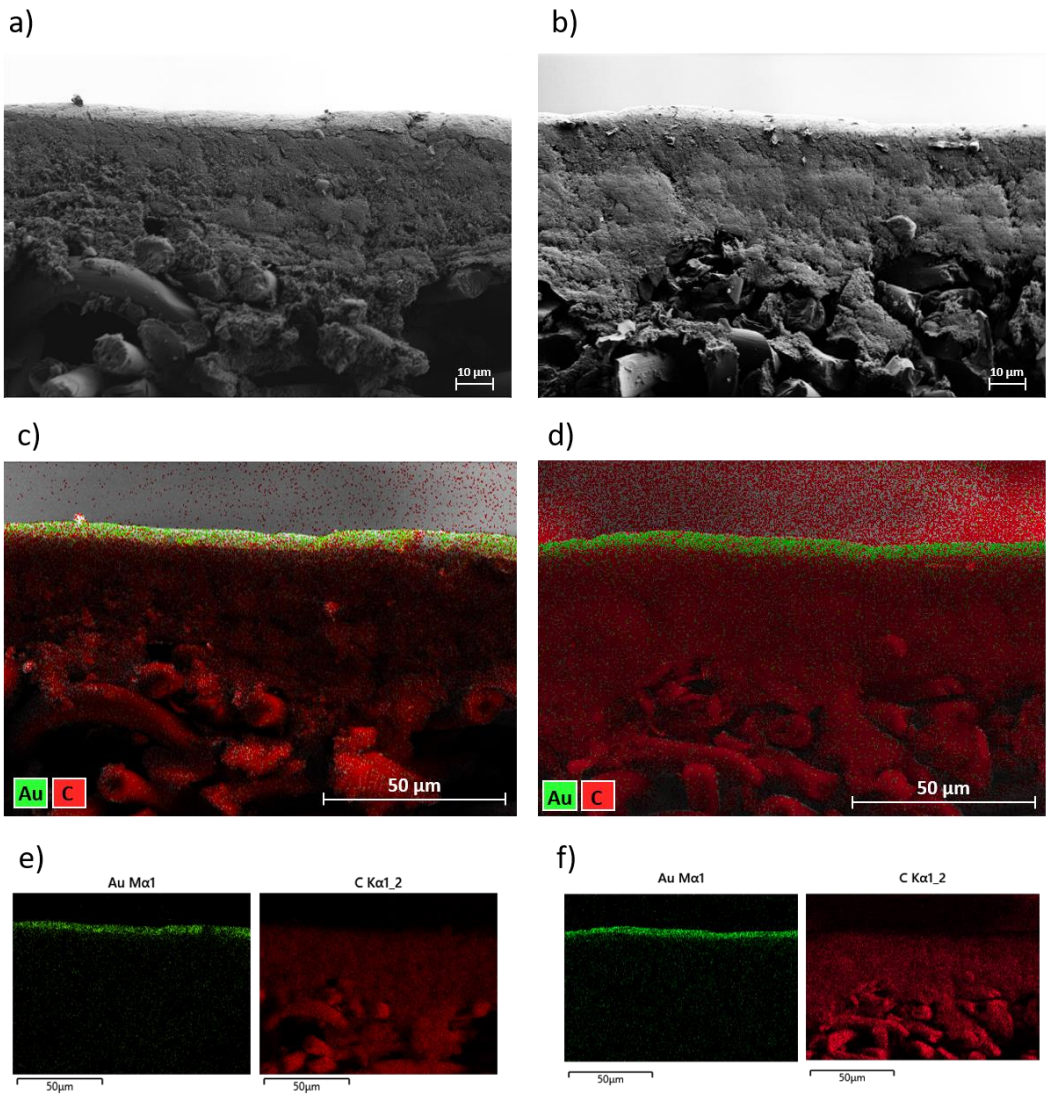

Figure 2. Representative cross-sectional SEM images (a and b) and EDX mapping (c, d, e, and f) of Au-PVP-free (a, c, and e), and Au-PVP (b, d, and f) GDEs. The Au loading was 50 μg_{Au} cm^{-2}.

3.1. Catalyst Screening Method Influence

Based on conventional H-cell measurements, Au is one of the most selective catalyst materials for the CO2RR to CO[14]. Therefore, we first investigated the Au-PVP-free catalyst in an H-cell setup to establish a benchmark performance. We chose a potential window for testing the CO2RR from -0.4 to -1.0 V_{RHE}. FEs and current densities of the gaseous products obtained from the CO2RR on

an electrode with 50 μg_{Au} cm^{-2} of Au-PVP-free catalyst are shown in Figure 3. The known behavior of Au catalyst is confirmed for low overpotentials. At -0.4 V_{RHE} the FE (faraday efficiency) for CO (FE_{CO}) is almost 100 %. However, at the same time, the current density is only around 20 mA cm^{-2}. Decreasing the applied potential to -0.7 V_{RHE} and -1.0 V_{RHE}, the total current density increases to around 40 and 80 mA cm^{-2}, respectively. However, at the same time, the FE_{CO} decreases to 90 and 75 %, respectively. This decrease in FE_{CO} might be in part due to the different availability of the two different reactants CO_2 and water. Furthermore, a slight time dependence in the recorded FE_{CO} and total current density is seen. Yet, under none of the investigated conditions, the total current densities in the H-cell setup reach the commercially relevant values of ≈200 mA cm^{-2} [9].

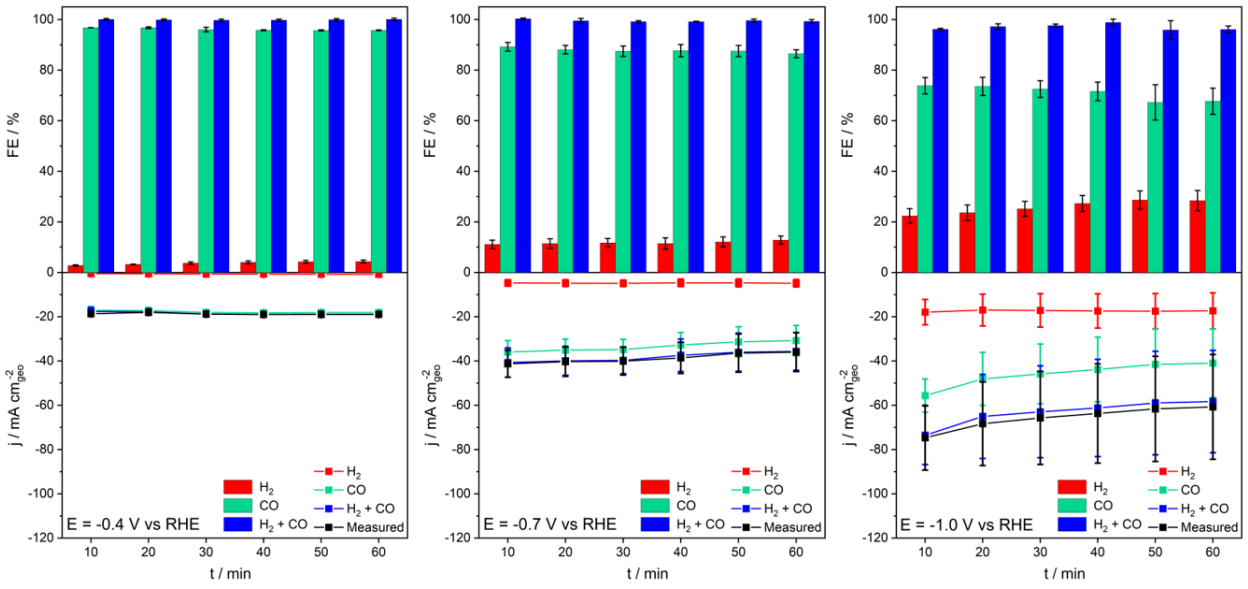

Figure 3. FEs and current densities of the gaseous products obtained from CO2RR on 50 μg_{Au} cm^{-2} of Au-PVP-free catalyst every 10 min of 1-hour CO_2 electrolysis at different applied potentials in an H-Cell setup. The solid lines are guides for the eye to better follow the trends. The error bars indicate the standard deviation retrieved from three measurements.

Commercially more relevant current densities can be obtained in GDE setups, where the reactant gas does not need to be first dissolved in liquid electrolyte. To demonstrate this influence, we performed the same CO2RR studies in our recently introduced zero-gap, half-cell GDE setup[8,36] setup instead of the H-cell setup. The obtained FE_{CO} and current densities are shown in Figure 4 and Figure S9. It is seen that by supplying a continuous CO_2 stream through the GDL to the catalyst layer in GDE setup, the total current densities could be increased to ca. 50, 160, and 250 mA cm^{-2} at -0.4, -0.7 and -1.0 V_{RHE}, respectively. In the latter case, the current density achieves the industrially relevant 200 mA cm^{-2}, however, this achievement is clearly at the expense of selectivity towards CO. With increasing total current densities, the FE_{CO} decreases from ca. 65 % to 50 % and 40 %. Furthermore, at higher overpotentials, neither the total current densities nor the FE_{CO} are stable but decay within the 1 h of the measurement. It has been shown previously that without the direct presence of a solid-supported electrolyte, the CO_2 reduction selectivity can be heavily penalized[43,44]. As a general observation, it can be stated that in the H-cell as well the GDE setup, the FE_{CO} decreases with increasing overpotential and concomitant increasing total current density. Furthermore, it is seen that the higher total current densities achieved (at the same potential) in the GDE are penalized by a lower selectivity towards CO (FE_{CO}). These results could indicate that the selectivity depends also on the current density and not only the overpotential.

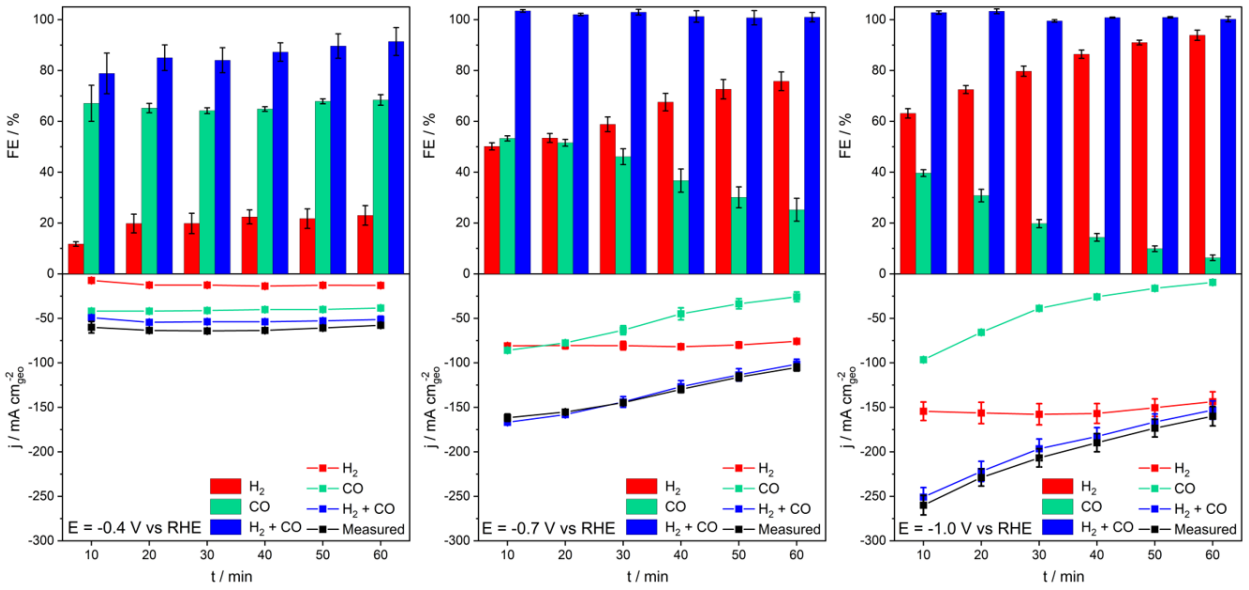

Figure 4. FEs and current densities of the gaseous products obtained from CO2RR on 50 μg_{Au} cm^{-2} of Au-PVP-free catalyst every 10 min of 1-hour CO_2 electrolysis at different applied potentials in GDE setup. The solid lines are guides for the eye to better follow the trends.

3.2. Loading Effect in GDE setup

Another influence of the FEs and total current densities can be expected from the catalyst loading on the GDE. In Figure S10 the results obtained from a GDE with 10 μg_{Au} cm^{-2} of Au-PVP-free catalyst are shown and in Figure 5 we compare the different loadings of the Au-PVP-free catalyst in the GDE setup. It is observed that by decreasing the loading of the catalyst from 50 to 10 μg_{Au} cm^{-2}, the selectivity towards CO worsens. However, the change in current densities is almost negligible. This indicates that the selectivity of the Au-PVP-free catalyst might depend on the current density per metal loading.

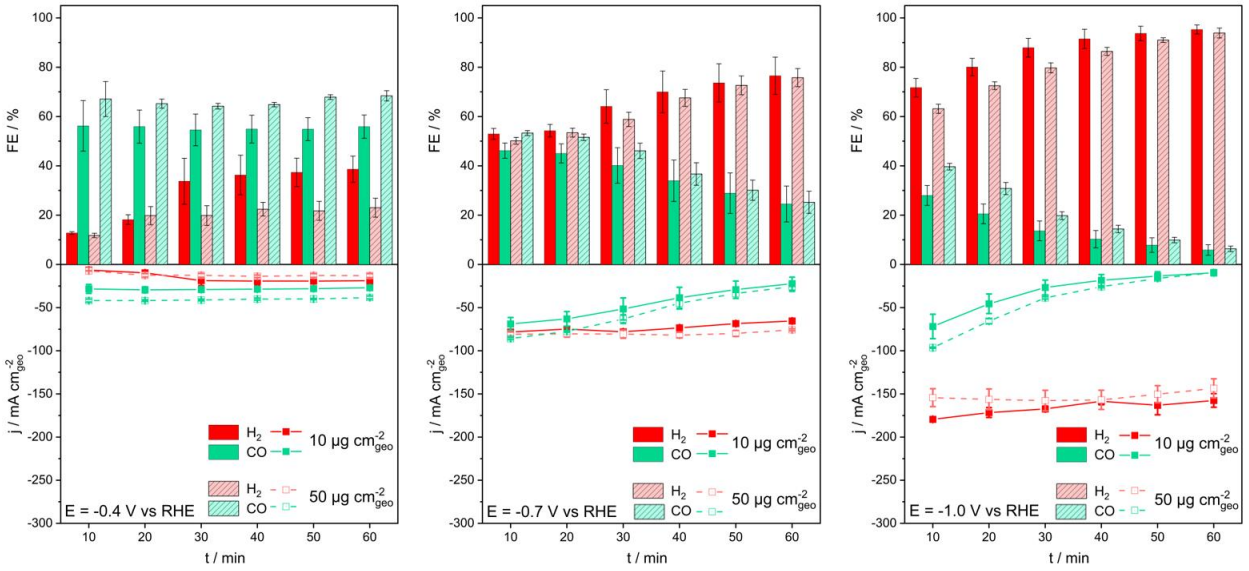

Figure 5. FEs and current densities of the gaseous products obtained from CO2RR on 10 and 50 μg_{Au} cm^{-2} of Au-PVP-free catalyst every 10 min of 1-hour CO_2 electrolysis at different applied potentials in the GDE setup. The solid lines are guides for the eye to better follow the trends.

3.3. PVP Influence

After scrutinizing the influence of the setup and metal loading on the performance with Au-free-PVP NPs, we investigated the influence of PVP on the achieved current densities and FE_{CO}. In Figures 6 (see also Figure S11-12) we compare the influence of PVP in the GDE setup. As mentioned in the introduction, surfactants, and capping agents such as PVP are often employed in the synthesis of NPs, especially if shape-control is desired. Their use in catalysis, however, often requires their removal from the metallic surfaces without loss of surface quality[30]. Besides this practical implication, it has been shown that ligand-free Au NPs show far better agreement between theory and experiment (in a Langmuir-Hinshelwood-model reduction reaction) compared to polymer-capped AuNPs, attributed to the higher surface potential and higher accessibility of active sites[35]. Our electrochemical results show that in the presence of PVP at low

overpotential (-0.4 V_{RHE}), the total FE is substantially lower than in the measurements of the Au-PVP-free catalyst. Furthermore, a constant increase in total FE can be observed, which indicates an electrochemical cleaning of the Au-PVP catalyst, i.e., the desorption of the PVP from the catalyst surface. Such a process would be in line with the decreasing cell resistance observed during the measurement (Figure S14), which can be an indication of the electrochemical cleaning of the PVP. To determine if the PVP is only partially or completely removed from the catalyst surface, we performed Raman spectroscopy before and after CO2RR. The Raman spectra of (1) PVP powder, (2) Au-PVP ink on mica film, (3) the blank GDL, (4) pristine Au-PVP catalyst loaded with 50 μg_{Au} cm^{-2} on a GDL, and (5) resembling (4) after 1 hour of electrolysis at -1.0 V_{RHE} are shown in the Figure S15. Although we could detect a sharp PVP signal in the Raman spectrum of the Au-PVP ink on a mica film, due to the lack of enough Au-PVP catalyst on the GDL, we were not even able to detect a clear PVP signal in the pristine sample.

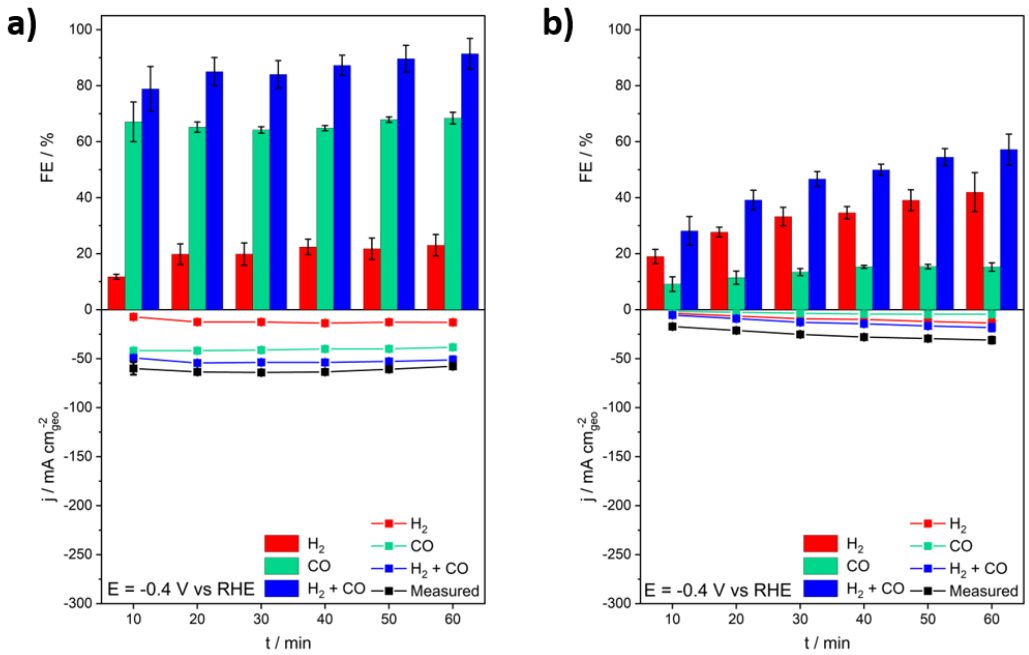

Figure 6. FEs and current densities of the gaseous products obtained from CO2RR on 50 μg_{Au} cm^{-2} of a) Au-PVP-free b) Au-PVP catalyst every 10 min of 1-hour CO_2 electrolysis at -0.4 V vs RHE applied potentials in the GDE setup. The solid lines are guides for the eye to better follow the trends.

To complete our comparison, we investigated the influence of PVP in a H-Cell setup (Figure 7 and Figure S13). As for the case of the Au-PVP-free catalyst, the FE_{CO} is improved in the direct presence of the aqueous electrolyte in the H-cell setup, but this improvement is at the expense of the lower current densities as compared to the GDE setup. As in the GDE setup, in the presence of the PVP a lower total FE in the beginning of the 1-hour CO_2 electrolysis was observed in H-Cell setup. However, the detrimental effect of PVP on the FE is substantially less severe than in the GDE setup.

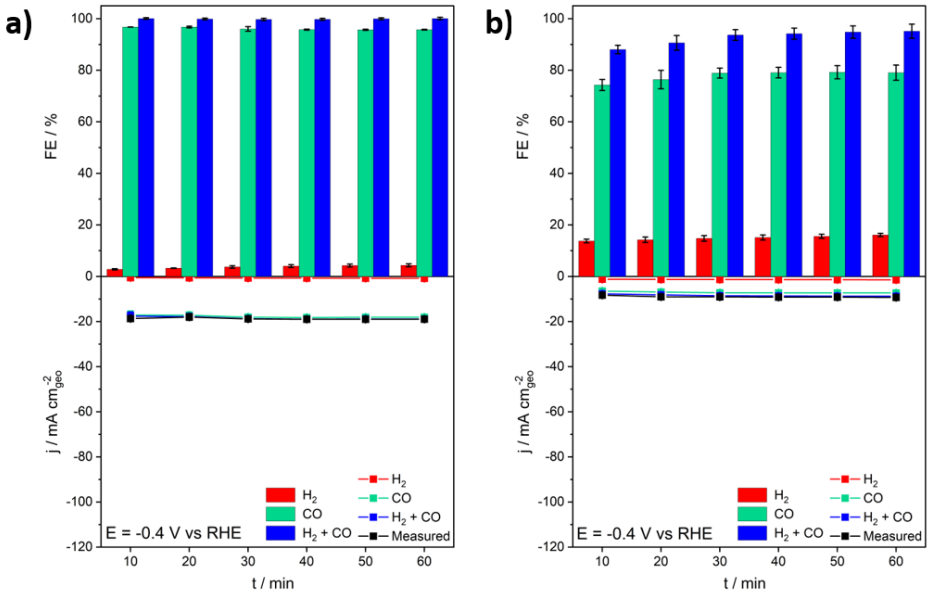

Figure 7. FEs and current densities of the gaseous products obtained from CO2RR on 50 μg_{Au} cm^{-2} of a) Au-PVP-free b) Au-PVP catalyst every 10 min of 1-hour CO_2 electrolysis at -0.4 V vs RHE applied potentials in H-Cell setup. The solid lines are guides for the eye to better follow the trends.

4. Conclusion

In this work, we systematically investigated the influence of three experimental variables on the performance of Au-based catalysts for the electrochemical CO2RR, i.e., first the influence of the reaction environment (testing setup), second the influence of the catalyst loading, third the absence or presence of a polymer surfactant. The electrocatalytic reaction was performed both in a conventional H-cell and a GDE setup, whereas the influence of surfactants was investigated by adding surfactants to a surfactant-free colloidal suspension of Au NPs. For all cases, we observed the known behavior of Au that is very selective towards CO in the CO2RR. Mimicking commercially relevant conditions for the CO2RR by using a zero-gap, half-cell GDE setup enables high mass transport conditions, we observed that technologically relevant total current densities higher than 200 mA cm^{-2} can be obtained which was not the case in an H-cell setup. However, the high current densities were achieved at the expense of a lower selectivity towards CO. The results also indicate that the selectivity of the CO2RR towards CO depends on the current density per metal loading, but increasing the catalyst loading from 10 to 50 μg_{Au} cm^{-2} only negligible improvements in the current densities are achieved. This result calls for effective catalyst benchmarking procedures as having been proposed in proton exchange membrane fuel cell research[45]. Last but not least, independent of the screening method, the presence of PVP inhibits CO as a reduction product. To maximize selectivity towards CO, the use of surfactants such as PVP in the catalyst synthesis should be avoided. The sensitivity of the catalyst to PVP inhibition seems more critical in a GDE setup than it is in an H-cell. This knowledge will be key to develop further CO2RR catalysts for industrial applications.

5. Acknowledgment

This work was supported by the Swiss National Science Foundation (SNSF) via project No. 200021_184742. Jonathan Quinson acknowledges the European Union's Horizon 2020 research and innovation program under the Marie Skłodowska-Curie grant agreement No. 840523 (CoSolCat). S. B. Simonsen and L. Theil Kuhn, Technical University of Denmark, are thanked for access to TEM. The Niels Bohr Institute, University of Copenhagen, Denmark, is thanked for access to SAXS equipment, in particular J. K. K. Kirkensgaard.

6. References

1. Whipple, D. T. & Kenis, P. J. A. Prospects of CO2 utilization via direct heterogeneous electrochemical reduction. *J. Phys. Chem. Lett.* **1**, 3451–3458 (2010).
2. Centi, G. & Perathoner, S. Opportunities and prospects in the chemical recycling of carbon dioxide to fuels. *Catal. Today* **148**, 191–205 (2009).
3. Hu, H. *et al.* Activation Matters: Hysteresis Effects during Electrochemical Looping of Colloidal Ag Nanowire Catalysts. *ACS Catal.* **10**, 8503–8514 (2020).
4. Verma, S. *et al.* Insights into the Low Overpotential Electroreduction of CO2 to CO on a Supported Gold Catalyst in an Alkaline Flow Electrolyzer. *ACS Energy Lett.* **3**, 193–198 (2018).
5. Hernández, S. *et al.* Syngas production from electrochemical reduction of CO2: Current status and prospective implementation. *Green Chem.* **19**, 2326–2346 (2017).
6. Verma, S., Kim, B., Jhong, H. R. M., Ma, S. & Kenis, P. J. A. A gross-margin model for defining technoeconomic benchmarks in the electroreduction of CO2. *ChemSusChem* **9**, 1972–1979 (2016).
7. Martín, A. J., Larrazábal, G. O. & Pérez-Ramírez, J. Towards sustainable fuels and chemicals through the electrochemical reduction of CO2: Lessons from water electrolysis. *Green Chem.* **17**, 5114–5130 (2015).
8. Gaìlvez-Vaìzquez, M. D. J. *et al.* Environment matters: CO2RR electrocatalyst performance testing in a gas-fed zero-gap electrolyzer. *ACS Catal.* 13096–13108 (2020) doi:10.1021/acscatal.0c03609.
9. Burdyny, T. & Smith, W. A. CO2 reduction on gas-diffusion electrodes and why catalytic performance must be assessed at commercially-relevant conditions. *Energy Environ. Sci.* **12**, 1442–1453 (2019).
10. Endrődi, B. *et al.* Continuous-flow electroreduction of carbon dioxide. *Prog. Energy Combust. Sci.* **62**, 133–154 (2017).
11. Jovanovic, S. *et al.* Post-Test Raman Investigation of Silver Based Gas Diffusion Electrodes.

J. Electrochem. Soc. **167**, 086505 (2020).
12. Vennekoetter, J. B., Sengpiel, R. & Wessling, M. Beyond the catalyst: How electrode and reactor design determine the product spectrum during electrochemical CO2 reduction. *Chem. Eng. J.* **364**, 89–101 (2019).
13. Delacourt, C., Ridgway, P. L., Kerr, J. B. & Newman, J. Design of an Electrochemical Cell Making Syngas (CO+H[sub 2]) from CO[sub 2] and H[sub 2]O Reduction at Room Temperature. *J. Electrochem. Soc.* **155**, B42 (2008).
14. Goyal, A., Marcandalli, G., Mints, V. A. & Koper, M. T. M. Competition between CO2Reduction and Hydrogen Evolution on a Gold Electrode under Well-Defined Mass Transport Conditions. *J. Am. Chem. Soc.* **142**, 4154–4161 (2020).
15. Turkevich, J., Stevenson, P. C. & Hillier, J. A study of the nucleation and growth processes in the synthesis of colloidal gold. *Discuss. Faraday Soc.* **11**, 55–75 (1951).
16. Komiyama, M. Design and Preparation of Impregnated Catalysts. *Catal. Rev.* **27**, 341–372 (1985).
17. Suchomel, P. *et al.* Simple size-controlled synthesis of Au nanoparticles and their size-dependent catalytic activity. *Sci. Rep.* **8**, 1–11 (2018).
18. Han, G. H., Lee, S. H., Seo, M. G. & Lee, K. Y. Effect of polyvinylpyrrolidone (PVP) on palladium catalysts for direct synthesis of hydrogen peroxide from hydrogen and oxygen. *RSC Adv.* **10**, 19952–19960 (2020).
19. Koczkur, K. M., Mourdikoudis, S., Polavarapu, L. & Skrabalak, S. E. Polyvinylpyrrolidone (PVP) in nanoparticle synthesis. *Dalt. Trans.* **44**, 17883–17905 (2015).
20. Johnson, P., Trybala, A., Starov, V. & Pinfield, V. J. Effect of synthetic surfactants on the environment and the potential for substitution by biosurfactants. *Adv. Colloid Interface Sci.* **288**, (2021).
21. Safo, I. A. & Oezaslan, M. Electrochemical Cleaning of Polyvinylpyrrolidone-capped Pt Nanocubes for the Oxygen Reduction Reaction. *Electrochim. Acta* **241**, 544–552 (2017).
22. Quinson, J., Kunz, S. & Arenz, M. Beyond Active Site Design: a Surfactant-Free Toolbox Approach for Optimised Supported Nanoparticle Catalysts. *ChemCatChem* **13**, 1692 – 1705 (2021).
23. Reichenberger, S., Marzun, G., Muhler, M. & Barcikowski, S. Perspective of Surfactant-Free Colloidal Nanoparticles in Heterogeneous Catalysis. *ChemCatChem* **11**, 4489–4518 (2019).
24. Zhang, J., Chen, G., Chaker, M., Rosei, F. & Ma, D. Gold nanoparticle decorated ceria nanotubes with significantly high catalytic activity for the reduction of nitrophenol and mechanism study. *Appl. Catal. B Environ.* **132**–**133**, 107–115 (2013).
25. Marshall, S. T. *et al.* Controlled selectivity for palladium catalysts using self-assembled monolayers. *Nat. Mater.* **9**, 853–858 (2010).
26. Pang, S. H., Schoenbaum, C. A., Schwartz, D. K. & Will Medlin, J. Effects of thiol modifiers on the kinetics of furfural hydrogenation over Pd catalysts. *ACS Catal.* **4**, 3123–3131 (2014).
27. Fernández, P. S. *et al.* Platinum nanoparticles produced by EG/PVP method: The effect of cleaning on the electro-oxidation of glycerol. *Electrochim. Acta* **98**, 25–31 (2013).
28. Li, D. *et al.* Surfactant removal for colloidal nanoparticles from solution synthesis: The effect on catalytic performance. *ACS Catal.* **2**, 1358–1362 (2012).
29. Cargnello, M. *et al.* Efficient removal of organic ligands from supported nanocrystals by fast thermal annealing enables catalytic studies on well-defined active phases. *J. Am.*

Chem. Soc. **137**, 6906–6911 (2015).
30. Hasché, F., Oezaslan, M. & Strasser, P. In situ observation of the thermally induced growth of platinum- nanoparticle catalysts using high-temperature X-ray diffraction. *ChemPhysChem* **13**, 828–834 (2012).
31. Amri, N. El & Roger, K. Polyvinylpyrrolidone (PVP) impurities drastically impact the outcome of nanoparticle syntheses. *J. Colloid Interface Sci.* **576**, 435–443 (2020).
32. Arminio-Ravelo, J. A. *et al.* Synthesis of Iridium Nanocatalysts for Water Oxidation in Acid: Effect of the Surfactant. *ChemCatChem* **12**, 1282–1287 (2020).
33. Amendola, V. *et al.* Room-Temperature Laser Synthesis in Liquid of Oxide, Metal-Oxide Core-Shells, and Doped Oxide Nanoparticles. *Chem. - A Eur. J.* **26**, 9206–9242 (2020).
34. Merk, V. *et al.* In Situ Non-DLVO Stabilization of Surfactant-Free, Plasmonic Gold Nanoparticles: E ff ect of Hofmeister ' s Anions. (2014).
35. Gu, S. *et al.* Ligand-free Gold Nanoparticles as a Reference Material for Kinetic Modelling of Catalytic Reduction of 4-Nitrophenol. *Catal. Letters* **145**, 1105–1112 (2015).
36. De Jesús Gálvez-Vázquez, M. *et al.* Testing a Silver Nanowire Catalyst for the Selective CO2 Reduction in a Gas Diffusion Electrode Half-cell Setup Enabling High Mass Transport Conditions. *Chimia (Aarau).* **73**, 922–927 (2019).
37. Wiberg, G. K. H., Fleige, M. & Arenz, M. Gas diffusion electrode setup for catalyst testing in concentrated phosphoric acid at elevated temperatures. *Rev. Sci. Instrum.* **86**, (2015).
38. Kohsakowski, S. *et al.* Effective size separation of laser-generated, surfactant-free nanoparticles by continuous centrifugation. *Nanotechnology* **31**, (2020).
39. Letzel, A. *et al.* Time and Mechanism of Nanoparticle Functionalization by Macromolecular Ligands during Pulsed Laser Ablation in Liquids. *Langmuir* **35**, 3038–3047 (2019).
40. Alinejad, S., Quinson, J., Schröder, J. J., Kirkensgaard, J. J. K. & Arenz, M. Carbon-supported platinum electrocatalysts probed in a gas diffusion setup with alkaline environment: How particle size and mesoscopic environment influence the degradation mechanism. *ACS Catal.* 13040–13049 (2020) doi:10.1021/acscatal.0c03184.
41. Alinejad, S. *et al.* Testing fuel cell catalysts under more realistic reaction conditions: accelerated stress tests in a gas diffusion electrode setup. *J. Phys. Energy* **2**, 024003 (2020).
42. Quinson, J. *et al.* Surfactant-free synthesis of size controlled platinum nanoparticles: Insights from in situ studies. *Appl. Surf. Sci.* **549**, (2021).
43. Li, Y. C. *et al.* Electrolysis of CO2 to Syngas in Bipolar Membrane-Based Electrochemical Cells. *ACS Energy Lett.* **1**, 1149–1153 (2016).
44. Salvatore, D. A. *et al.* Electrolysis of Gaseous CO2 to CO in a Flow Cell with a Bipolar Membrane. *ACS Energy Lett.* **3**, 149–154 (2018).
45. Gasteiger, H. A., Kocha, S. S., Sompalli, B. & Wagner, F. T. Activity benchmarks and requirements for Pt, Pt-alloy, and non-Pt oxygen reduction catalysts for PEMFCs. *Appl. Catal. B Environ.* **56**, 9–35 (2005).